Chinese Journal of Oceanology and Limnology
Vol. 33 No. 1, P. 262-271, 2015
http://dx.doi.org/10.1007/s00343-014-3338-5

Preliminary validation of SMOS sea surface salinity measurements in the South China Sea*

REN Yongzheng (任永政)[1, **], DONG Qing (董庆)[1], HE Mingxia (贺明霞)[2]

[1] *Key Laboratory of Digital Earth Science, Institute of Remote Sensing and Digital Earth, Chinese Academy of Sciences, Beijing 100094, China*

[2] *Ocean Remote Sensing Institute, Ocean University of China, Qingdao 266002, China*

Received Dec. 17, 2013; accepted in principle Jan. 27, 2014; accepted for publication Mar. 19, 2014

Abstract The SMOS (soil moisture and ocean salinity) mission undertaken by the European Space Agency (ESA) has provided sea surface salinity (SSS) measurements at global scale since 2009. Validation of SSS values retrieved from SMOS data has been done globally and regionally. However, the accuracy of SSS measurements by SMOS in the China seas has not been examined in detail. In this study, we compared retrieved SSS values from SMOS data with in situ measurements from a South China Sea (SCS) expedition during autumn 2011. The comparison shows that the retrieved SSS values using ascending pass data have much better agreement with in situ measurements than the result derived from descending pass data. Accuracy in terms of bias and root mean square error (RMS) of the SSS retrieved using three different sea surface roughness models is very consistent, regardless of ascending or descending orbits. When ascending and descending measurements are combined for comparison, the retrieved SSS using a semi-empirical model shows the best agreement with in situ measurements, with bias -0.33 practical salinity units and RMS 0.74. We also investigated the impact of environmental conditions of sea surface wind and sea surface temperature on accuracy of the retrieved SSS. The SCS is a semi-closed basin where radio frequencies transmitted from the mainland strongly interfere with SMOS measurements. Therefore, accuracy of retrieved SSS shows a relationship with distance between the validation sites and land.

Keyword: sea surface salinity (SSS); soil moisture and ocean salinity (SMOS); sea surface roughness model; South China Sea (SCS)

1 INTRODUCTION

Global measurements of sea surface height, sea surface temperature, and sea surface wind by spaceborne sensors have reached a mature level. Remote measurement of sea surface salinity (SSS) from space began to draw our attention when the Soil Moisture and Ocean Salinity (SMOS) mission and Aquarius were launched in November 2009 and June 2011 by the European Space Agency (ESA) and National Aeronautics and Space Administration (NASA), respectively. Seawater salinity is one of the most important parameters of marine environmental dynamics. Changes of salinity are closely related to the marine environment and global climate change. Remote sensing of SSS has a wide range of applications, such as the study of both large- and meso-scale phenomena and of nearshore marine environments. Both the SMOS and Aquarius satellites carry an L-band microwave radiometer. To obtain the radiation-signal precision and high spatial resolution data required for terrestrial and marine science applications, the single payload of SMOS (McMullan et al., 2008), the Microwave Imaging Radiometer with Aperture Synthesis (MIRAS), takes advantage of the technique of interferometric aperture synthesis in both the along- and across-track directions (Martín-Neira and Goutoule, 1997). The MIRAS instrument comprises 69 L-band radiometer receivers, of which

* Supported by the National Natural Science Foundation of China (Nos. 41006110, 41106155)
** Corresponding author: renyz@radi.ac.cn

54 are evenly distributed on three arms in a Y-shape, and 12 are placed in a central hub.

Based on the SMOS SSS Level 2 product (Zine et al., 2008) released by ESA, numerous assessment and validation tests have been conducted for global ocean and regional basins. Boutin et al. (2012) compared SSS measurements acquired between 29 July and 5 September 2010 with Argo measurements. They found that 10-day averaged SSS products of spatial resolution 100 km×100 km have an accuracy of 0.3–0.5 practical salinity units in terms of the standard deviation of ΔS (SSS_{SMOS}–SSS_{Argo}) in open water, and for sea surface wind speed of 3–12 m/s. Regional validation (Banks et al., 2012) shows that SMOS SSS products have good agreement with model simulation in the tropical/subtropical Atlantic. However, validation for the Indian Ocean (Subrahmanyam et al., 2013) indicates a large bias between the two. The three aforementioned validation exercises were conducted for SSS products acquired during a similar period, and they all indicated that biases of retrieved SSS data from SMOS ascending and descending passes were different. This may be attributed to inaccurate estimation of galactic glint, which was dominant during descending passes of the validation period (Reul et al., 2012).

The aforementioned validation exercises offer an overview of the quality of SMOS SSS products for global and regional basins. However, to our knowledge, validation of SMOS SSS data in the China Seas is not yet available. Very limited in situ measurements from Argo data of salinity in those seas are a major issue for the validation of SMOS products. If, as presently considered, SMOS measurements are strongly contaminated by radio-frequency interference in the China seas, the SSS product is not useful. However, accurate estimation of SSS in those seas is important, particularly the South China Sea (SCS). SSS is important in the water cycle, meso- and small-scale phenomena, nearshore marine science research, and marine environment protection. Therefore, in the present study, we present a preliminary validation of SMOS SSS products through a comparison with in situ measurements during an expedition in the SCS.

Following this introduction, we give a brief description of the geophysical models used to retrieve the SMOS SSS Level 2 product. In Section 3, the dataset used is described and post-processing of the Level 2 product is introduced. A comparison of that product with in situ measurements is detailed in Section 4. We also investigate the impact of environmental conditions on product accuracy. A discussion and conclusions are given in Section 5.

2 SEA SURFACE ROUGHNESS MODELS USED TO GENERATE SMOS SSS LEVEL 2 PRODUCT

The general principle for retrieving SSS from radiometer measurements is to generate a geophysical model that describes the relationship between brightness temperature and sea surface temperature (SST), SSS, radar incidence angle θ, and sea surface roughness parameter P_{rough}:

$$T_{\text{b, p}}(\theta,\text{SST},\text{SSS},P_{\text{rough}}) = T_{\text{b flat, p}}(\theta,\text{SST},\text{SSS}) + \Delta T_{\text{b rough, p}}(\theta,\text{SST},\text{SSS},\vec{P}_{\text{rough}}), \quad (1)$$

in which the brightness temperature of microwave radiation $T_{\text{b, p}}$ can be expressed as the sum of two temperatures, namely, brightness temperature of the calm sea surface $T_{\text{b flat, p}}$ and the excess brightness temperature $\Delta T_{\text{b rough, p}}$ caused by sea surface roughness. Here, p represents polarization. $T_{\text{b flat, p}}$ is described in detail by the Fresnel equation. The critical requirement for estimating brightness temperature is to resolve the contribution from the rough sea surface. Various studies (Dinnat et al., 2003; Reul et al., 2006) have compared the difference of SSS calculated by different sea surface roughness models, indicating that sea surface roughness models can lead to certain errors of SSS retrieval. In processing of the SMOS SSS product, three different sea surface roughness models were used to retrieve SSS, as described briefly below.

Model 1 uses the two-scale method to solve electromagnetic scattering and a doubled Durden and Vesecky spectrum to describe sea surface roughness (Wentz, 1975; Durden and Vesecky, 1985; Yuhe, 1997; Dinnat et al., 2002).

Model 2 uses small slope approximation emission theory (Irisov, 1997; Johnson and Zhang, 1999) and the Kudryavtsev wave spectrum (Kudryavtsev et al., 1999). This model divides the sea surface into non-bubble and bubble zones. For the bubble zone, a bubble emissivity model calculates sea surface emissivity. When the wind velocity at the sea surface is greater than 10–12 m/s, the effect of bubbles on sea surface emissivity is significant (Reul and Chapron, 2003).

Model 3 is a semi-empirical formula that was developed using measured emission-rate data of an L-band polarized sea surface in a Mediterranean experiment as well as oceanographic and

meteorological parameters (Camps et al., 2004; Gabarró et al., 2004). The model has been used in the inversion of airborne radiometer SSS data, under a variety of sea conditions.

Through the input of additional data including sea surface temperature, sea surface wind field, and the initial SSS estimate, one can simulate brightness temperature according to Eq.1. Taking into account polarizations and imaging geometries, the SMOS SSS processor subsequently converts the simulated brightness temperature to the brightness temperature that should be measured by the SMOS satellite under the initial conditions. By comparing the simulated brightness temperature with actual SMOS measurement, the initial SSS is adjusted via iteration until that temperature is consistent with that measured by SMOS.

3 DATASET

3.1 SMOS SSS Level 2 product

The SMOS SSS Level 2 product used herein is generated by the ESA L2OS processor (Version 5.5). The accessed SMOS SSS Level 2 product includes three values retrieved using the three sea surface roughness models described above. The swath of a single track is 600 km. During the expedition between August 21 and September 27, 2011, a total of 70 scenes of SMOS data were obtained for validation. There are numerous localized missing data in the Level 2 product. These missing data are mainly from contaminated brightness temperature measurements because of radio frequency interference. These were therefore flagged as poor quality data, which were removed before using the dataset.

To reduce uncertainties of the delivered SSS product, we applied both temporal and spatial averaging. We first applied a weekly average to the accessed SSS data. Then, a spatial filter of 4×4 window was used to reduce noise in the temporally averaged product. Subsequently, the smoothed data were linearly interpolated onto a 0.05°×0.05° grid. In addition, to investigate the effect of grid size on SSS accuracy, we averaged the data further onto a larger grid of 1°×1°. Figure 1 shows the weekly averaged (September 14–20) SSS data on the 0.05°×0.05° grid over the SCS. From left to right panels, the three columns are SSS values retrieved using different sea surface roughness models. From upper to lower panels, the three rows are SSS values derived from ascending, descending, and combined passes. The plot indicates that the SSS retrieved using the three sea surface roughness models differed only slightly when considering the ascending and descending data separately. However, there was a major discrepancy of SSS between ascending and descending passes, revealing a contrasting trend. If both ascending and descending data are used, a smooth (lower panel) SSS map is obtained, which shows that SSS in the SCS was greater than 33 psu during the week.

3.2 In situ measurements

In this study, all field salinity measurements were obtained during an expedition in autumn 2011. The expedition consisted of two legs; the first was in the northern SCS from August 21 to September 5, 2011, and the second was in the central and southern SCS from September 6 to October 3, 2011. Locations of thesampling stations are shown in Fig.2.

A Seabird CTD profiler was used to measure water salinity. To ensure accurate measurements for more than a hundred experiments over a long period, we used two CTDs (a SBE 911 plus CTD and SBE 19 plus CTD) to measure profiles of water salinity and water temperature at each station. For each experiment, we compared measurements from both CTDs and confirmed that there was no error introduced by instruments or operations. Then, an average value from the two measurements was used for comparison at each station. Figure 3 shows profiles of water temperature (left) and water salinity (right) measured by both CTDs at station No. 4 (22.268°N, 118.353°E). The results show identical measurements by the two profilers.

At each station, we also measured wind speed at a height of 10 m. Figure 4 shows time series of sea surface temperature and wind speed during the expedition. During the experimental period, the sea surface temperature was between 28°C and 31°C. All sea surface wind speeds were less than 12 m/s. This is considered a suitable condition for SSS retrieval from SMOS measurements, since Yin et al. (2012) found a large difference between simulated and empirical results for sea surface wind speed exceeding 12 m/s.

4 COMPARISON OF SMOS SSS WITH IN SITU MEASUREMENTS

Here, SMOS SSS data averaged at different grid sizes, derived from ascending and descending passes, as well as those retrieved using various sea surface roughness models, are compared with in situ measurements.

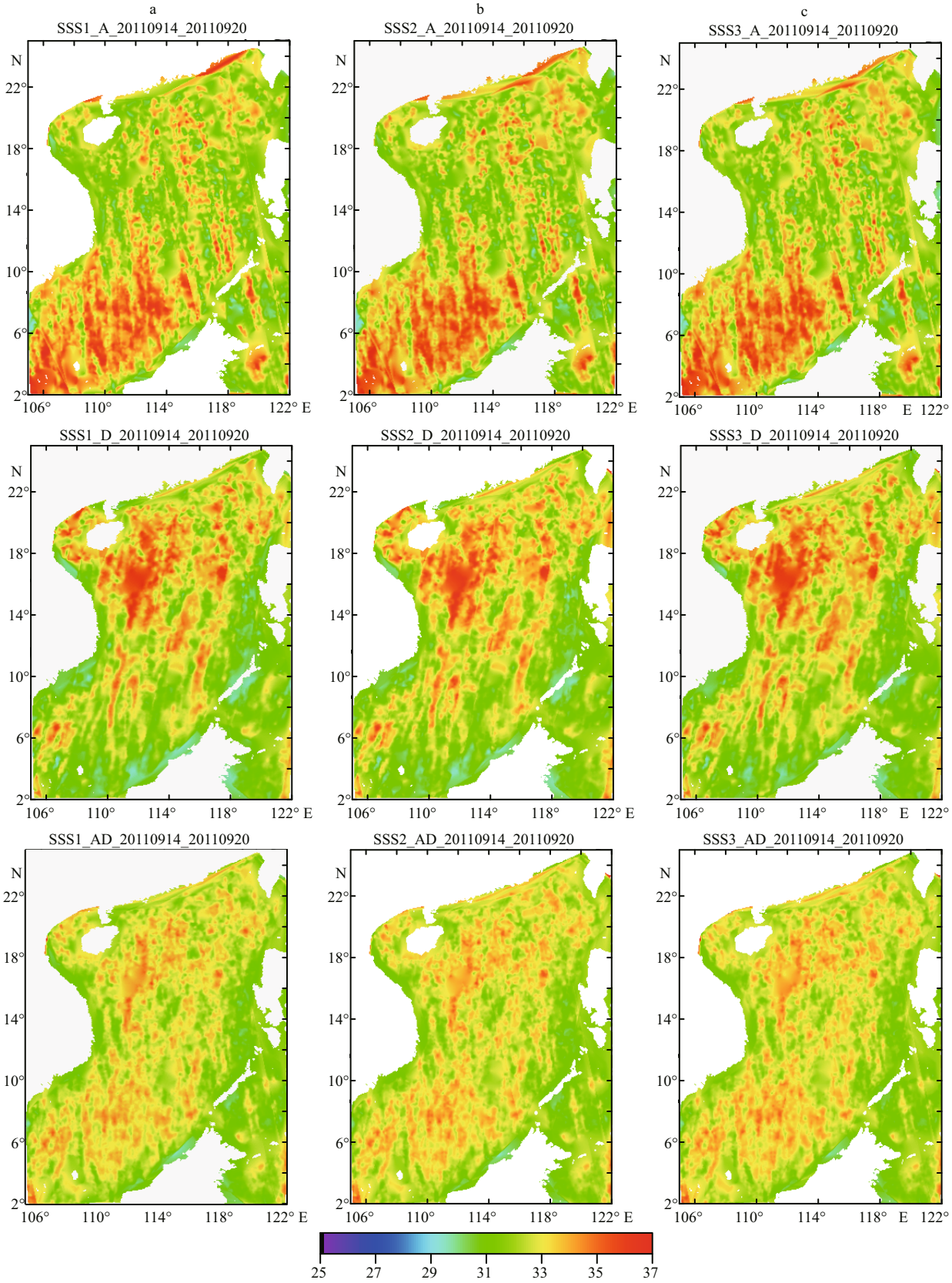

Fig.1 Distribution of weekly average SMOS SSS over SCS for September 14–20, 2011

Upper three figures show results of ascending orbit data, middle three show results of descending orbit data, and lower three results corresponding to all data. a. Weekly average SSS of Model 1; b. weekly average SSS of Model 2; c. weekly average SSS of Model 3.

4.1 Result

We first compared the weekly average SSS product on the 0.05°×0.05° grid with CTD measurements (Fig.5). As in Fig.1, from left to right panels, the diagrams compare SSS retrieved using the three sea surface roughness models. The upper, middle, and lower panels compare the ascending, descending, and combined SSS data, respectively. Statistical parameters for these comparisons are also listed in Table 1. The SSS derived from the ascending data show much better agreement with in situ measurements than those derived from the descending data. The discrepancy between the ascending and descending passes exceeds 0.5 and 0.3 for bias and RMS, respectively. The three models of sea surface roughness yielded very similar retrievals for both ascending and descending data. Model 2 functioned best for the ascending data, with bias only -0.1. However, the best retrieval for the descending data using Model 3 had a large and negative bias, at -0.71. If the ascending and descending SMOS products were used together, the optimal bias and RMS were -0.43 and 0.80, respectively.

To analyze the effect of spatial resolution on accuracy of the weekly average SMOS SSS, the products were further averaged to grid size 1°×1°. Figure 6 compares these values with in situ measurements. Compared to Fig.5, the SSS product averaged over the larger grid had better agreement with field measurements than that of the smaller grid, for both ascending and descending passes. In contrast to the comparison for SSS products averaged on the small grid, the ascending SSS product retrieved using

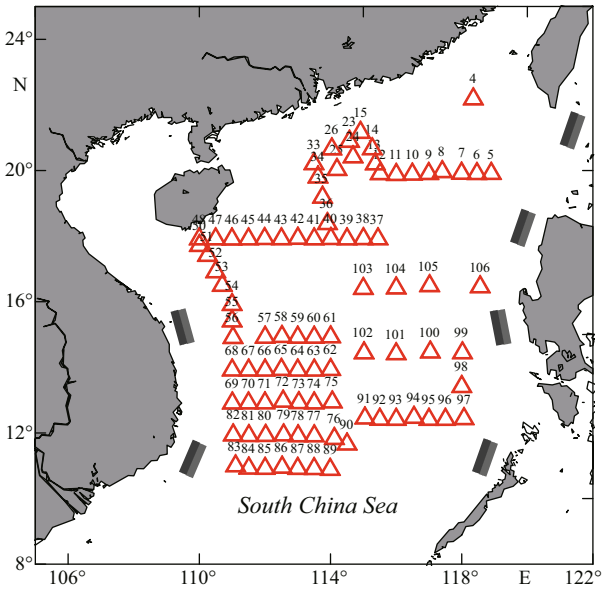

Fig.2 Map showing station locations for expedition in South China Sea during autumn 2011

Sponsored by China Natural Science Foundation (August 21–October 3, 2011).

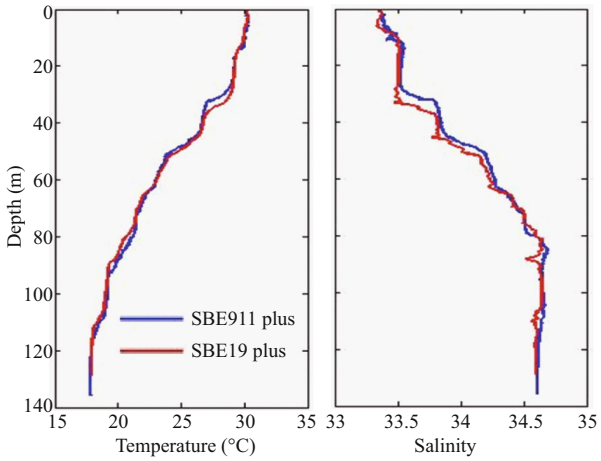

Fig.3 Temperature and salinity profiles measured using SBE 911 plus CTD and SBE 19 plus CTD instruments at No. 4 station (22.268°N, 118.353°E)

Red curve shows measurements from SBE 19 plus CTD. Blue curve shows measurements from SBE 911 plus CTD. Data were collected on August 23, 2011 at 22:47 UTC.

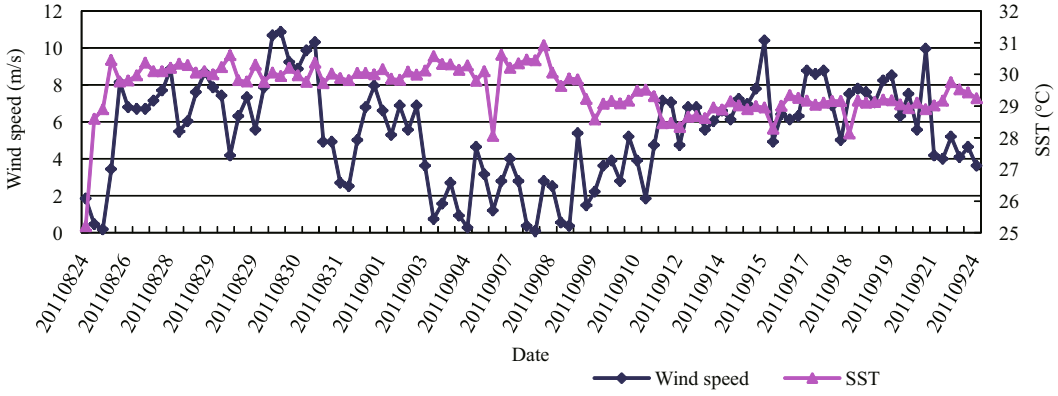

Fig.4 Time series of measured sea surface temperature and wind speed during expedition in SCS during autumn 2011

Table 1 Comparison between weekly average SSS data and in situ measurements

Sea surface roughness model		Bias	RMS	Sea surface roughness model		Bias	RMS
Ascending pass 0.05°×0.05°	Model 1	-0.141	0.979	Ascending pass 1°×1°	Model 1	-0.065	0.828
	Model 2	-0.100	0.928		Model 2	-0.045	0.845
	Model 3	-0.137	0.941		Model 3	0.003	0.782
Descending pass 0.05°×0.05°	Model 1	-0.720	1.280	Descending pass 1°×1°	Model 1	-0.730	1.092
	Model 2	-0.756	1.279		Model 2	-0.764	1.069
	Model 3	-0.706	1.248		Model 3	-0.736	1.082
Ascending and descending passes 0.05°× 0.05°	Model 1	-0.469	0.851	Ascending and descending passes 1°×1°	Model 1	-0.361	0.774
	Model 2	-0.464	0.814		Model 2	-0.374	0.779
	Model 3	-0.428	*0.795*		Model 3	-0.333	*0.739*

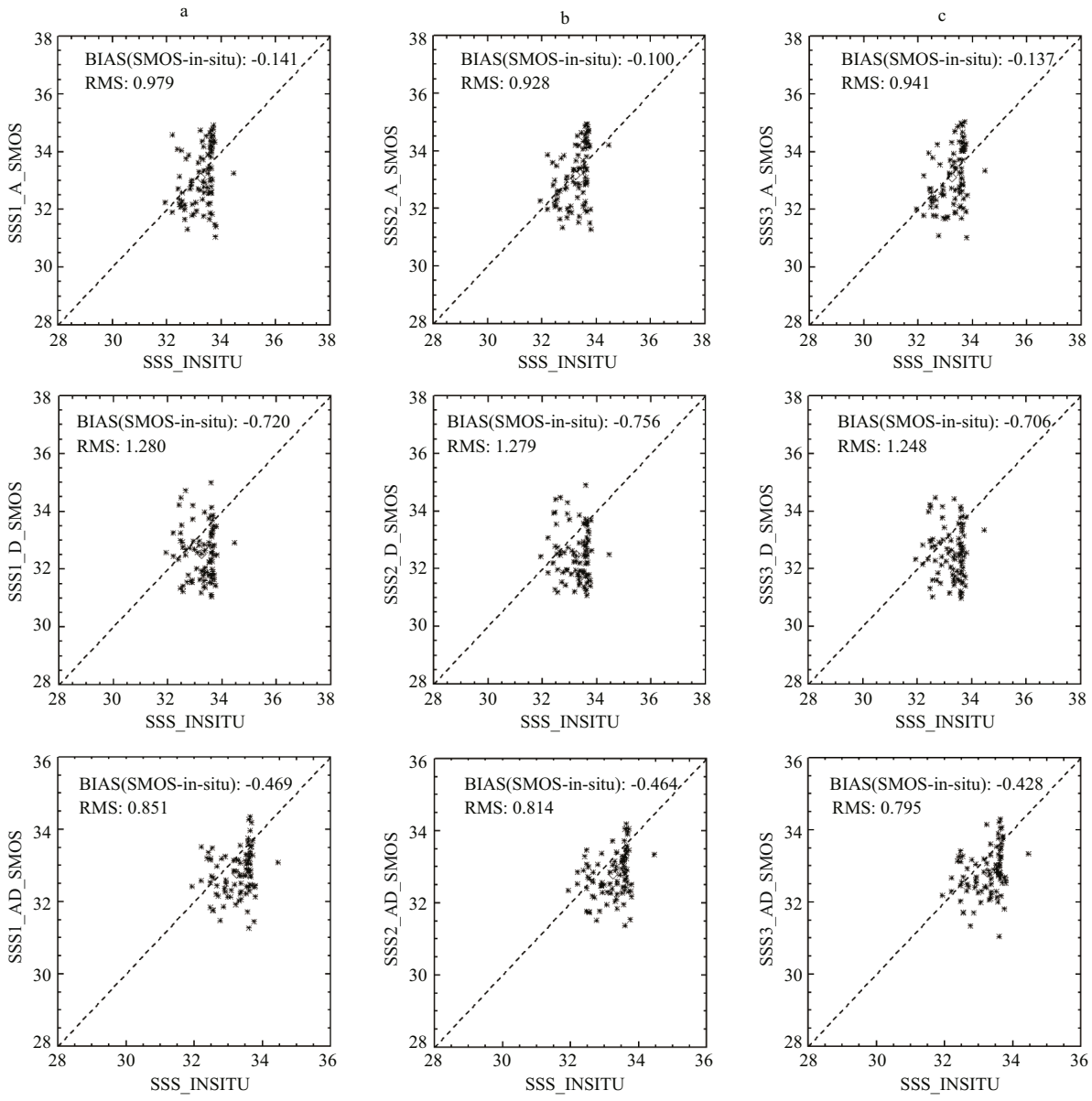

Fig.5 Comparison between weekly average SMOS SSS data and in situ measurements

Upper three figures show comparison of ascending orbit data, middle three a comparison of descending orbit data, and lower three figures a comparison of all data. Spatial resolution of SMOS salinity data was 0.05°×0.05°. Panels show (a) Model 1, (b) Model 2, and (c) Model 3.

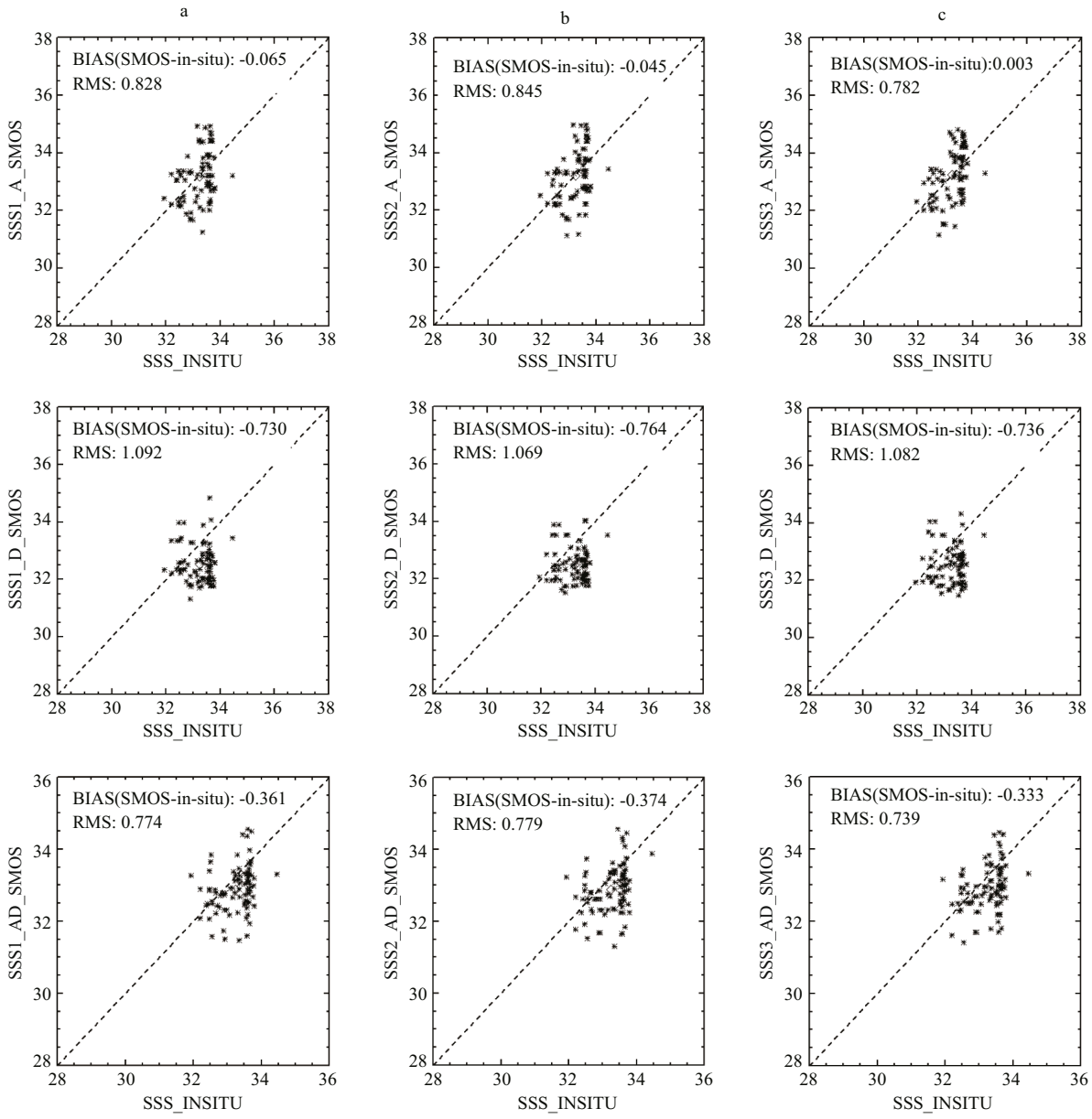

Fig.6 Same as Fig.5, but for SMOS SSS averaged on 1°×1° grid

Model 3 and averaged on the 1°×1° grid had the best agreement with in situ measurements, with zero bias and RMS of 0.78.

The above comparisons reveal that the SSS retrieved from ascending data is significantly superior to that from descending orbit data, regardless of sea surface roughness model used for retrieval and grid size used for averaging. Therefore, the discrepancy between the ascending and descending SSS products should stem from the SMOS brightness temperature measurement. When the SSS product was spatially averaged on the 1°×1° grid, accuracy systematically improved. This indicates that spatial averaging can reduce bias in the SSS product, induced either by the retrieval process or original measurement of brightness temperature by SMOS.

In the following section, we investigate whether environmental factors influenced accuracy of the SMOS SSS product. Because the SSS derived from ascending data had the best performance, error analysis focuses on these values.

4.2 Impact of environmental factors on SSS accuracy

Equation 1 indicates that sea surface temperature is a key factor for retrieval from the radiometer. Moreover, sea surface wind speed is important in the sea surface roughness model, which is also included in Eq.1. Therefore, we first analyzed the impact of

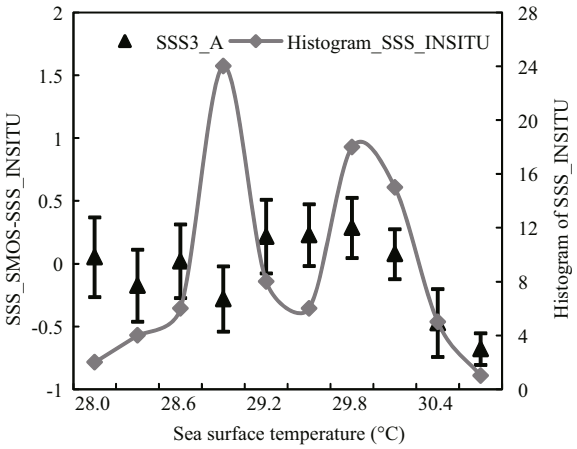

Fig.7 Distribution of mean error±standard deviation of retrieval results for ascending orbit data of Model 3 as a function of sea surface temperature measurements

Gray curve is histogram of in situ SSS values.

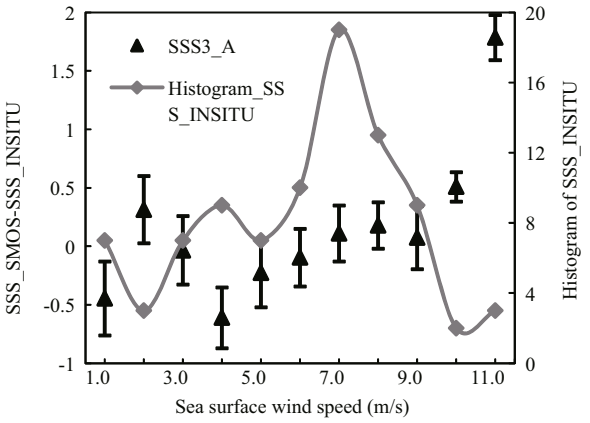

Fig.8 Distribution of mean error±standard deviation of retrieval results for ascending orbit data of Model 3 as a function of sea surface wind speed

Gray curve is histogram of in situ SSS values.

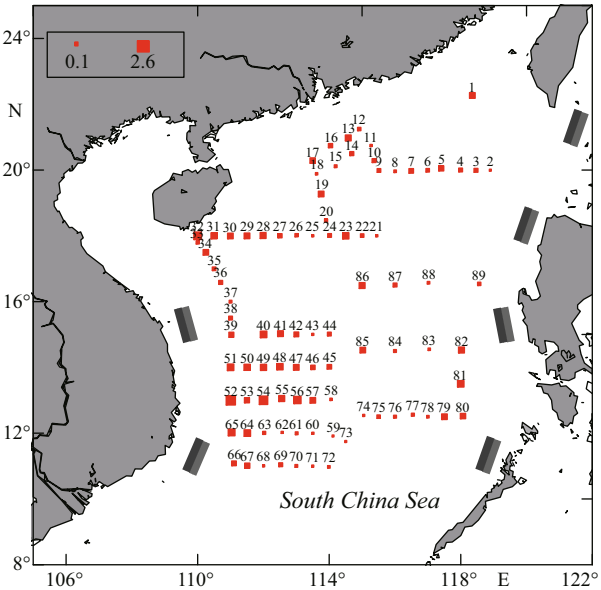

Fig.9 Distribution of mean error of SSS retrieved from ascending data of roughness Model 3

these two environmental factors on accuracy of the SSS level 2 products.

4.2.1 Impact of sea surface temperature

Error bars shown in Fig.7 indicate that the mean difference of SSS derived from the SMOS data and in situ measurements was within ±0.5 for sea surface temperatures 28–30°C. The substantial underestimation of SMOS SSS for sea surface temperatures greater than 30°C may be attributed to limited sampling measurements. We therefore conclude that the bias of SMOS SSS has no significant dependence on sea surface temperature in the range 28–30°C.

4.2.2 Impact of sea surface wind speed

The bias of SMOS SSS was random for sea surface wind speeds less than 3 m/s (Fig.8). From 4 to 10 m/s, the bias showed a slight trend approaching the in situ measurement with increased wind speed. For sea surface wind speeds greater than 10 m/s, it is difficult to derive the trend of bias related to wind speed, owing to limited data pairs. Nevertheless, we conclude that SSS retrieved from SMOS measurements has good accuracy, on the order of 0.5 for sea surface wind speeds between 3 m/s and 10 m/s.

4.2.3 Radio frequency interference (RFI)

RFI from land is considered a strong contamination source regarding SMOS measurements, which significantly limits exploitation of SMOS SSS products in the China seas. The SCS is surrounded by several countries, and RFI mainly originates from the land. Thus, we used the variation of bias along with distances between field stations and the mainland to identify the impact of RFI contamination on SMOS SSS products.

Figure 9 shows bias of retrieved and measured SSS at various field stations. Roughly, the accuracy of SMOS SSS is low in water regions close to southern Vietnam, Hainan Island of China, and south of the Philippines. In fact, SSS had good accuracy in the northern SCS, although the sampled points are near major population centers in southern China, such as Macau, Hong Kong, and Guangdong Province. SSS retrieved from SMOS measurements in the central SCS, far from the mainland, are clearly in close agreement with in situ measurements.

In Fig.10a and 10b, RFI data (released by the Centre d'Etudes Spatiales de la BIOsphère (CESBIO) research

team) from August 26 through September 9, 2011, are shown for ascending and descending passes, respectively. Both maps indicate that the RFI magnitude was indeed very strong in China. This magnitude also had significant temporal variation between ascending and descending passes. Although we were unable to obtain detailed RFI data, we found that the RFI had smallest magnitude at the center of the SCS, consistent with the bias map (Fig.9). We also see that RFI was smaller in the SCS than in other China seas, such as the East China and Yellow Seas. This indicates that the SMOS SSS level 2 product is applicable to the SCS.

5 DISCUSSION AND CONCLUSION

The SCS is a semi-enclosed area with complex environmental conditions. The suitability of ESA SMOS salinity products for the SCS has not been previously verified. Owing to a lack of Argo data, expeditions in the SCS were conducted to obtain in situ measurements of water salinity for validation.

Because three SSS values retrieved using different sea surface roughness models are provided in the ESA SSS level 2 products, we made comparisons. For weekly average SSS products on a 0.05°×0.05° grid, Model 2 yielded the best agreement with in situ measurements, with bias -0.10 for ascending orbit data. The SSS had the best result, with bias -0.71, for descending orbit data when Model 3 was used as the sea surface roughness model. When the SSS was further averaged on a larger grid size 1°×1°, agreement between the retrieved and measured SSS was further improved. The best result for the ascending orbit was zero bias and 0.78 psu for RMS with use of Model 3.

When the ascending and descending measurements were combined, Model 3 produced the best results among the three sea surface roughness models, with bias -0.43 and RMS 0.80 for the 0.05°×0.05° grid size and -0.33 and 0.74 for the 1°×1°grid.

Following the comparison, we analyzed the impact of sea surface temperature and wind speed on accuracy of the SMOS SSS level 2 product. Bias between the retrieved and measured SSS was ±0.5 and had no significant dependence on sea surface temperature in the range 28–30°C. For sea surface wind speeds between 3 m/s and 10 m/s, the retrieved SSS had close agreement with the in situ measurements, with a bias of ±0.5 too. We also investigated land contamination, including from the land itself and from land-based sources, on the SSS products. The retrieved SSS had the best accuracy at the center of the SCS. The largest bias was in water regions near

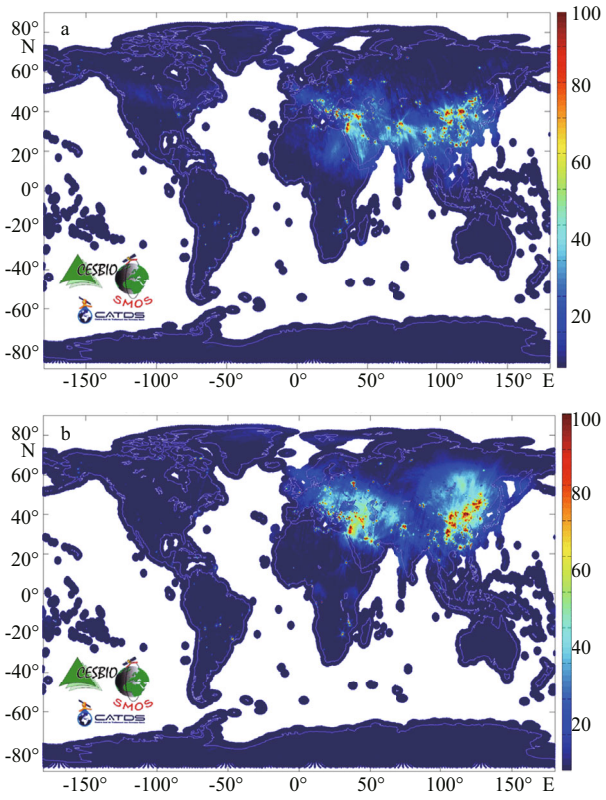

Fig.10 Distribution of 15-day SMOS RFI data

a. Ascending orbit data; b. descending orbit data (August 26–September 9, 2011) (©CESBIO)

southern Vietnam, Hainan Island of China, and the southern Philippines. This finding is consistent with the distribution of RFI in the SCS.

One distinguishing feature in the comparisons is asymmetry between the ascending and descending orbits. Our experiment showed that the discrepancy between the two passes exceeded 0.5 in terms of bias. Potential reasons for the asymmetry are contamination from RFI, galactic noise, and sun position with respect to the satellite (Font et al., 2010). Although it is difficult to investigate such reasons in this study, based on validation and error analysis, we recommend using the SMOS SSS level 2 products from ascending orbits for the SCS in future studies.

Boutin et al. (2012) verified the SMOS salinity products and demonstrated that under the conditions of open water, moderate wind speed, and spatial resolution 100 km×100 km, the standard deviation of SSS retrieved from ascending orbits and averaged over 10 days was 0.3–0.5. In the present study, in the semi-enclosed SCS, for wind speeds 0–11 m/s and spatial resolution 100 km×100 km, accuracy of the 7-day average SSS retrieved using Model 3 was 0.6–0.7 in terms of standard deviation. This is near the overall quality of the SSS level 2 product in the global ocean.

Validation of the SMOS SSS in the China seas was often excluded in earlier global validations. Our study shows that the quality of the SSS level 2 product for the SCS is comparable with that in the global ocean. This may offer an opportunity for further studies of SSS measurements from space for the China seas.

The SMOS SSS level 2 product used in the present study was generated by the ESA L2OS processor (Version 5.5). The newest L2OS processor is version 06.11, released on December 12, 2013. Results might change if the SSS products are obtained via the new processor. In addition, considering that brightness temperature measurement is very important to accurate SSS retrieval, simulation and validation of that temperature should be done in future studies.

6 ACKNOWLEDGMENT

The SMOS SSS data are provided by ESA.

References

Banks C J, Gommenginger C P, Srokosz M A, Snaith H M. 2012. Validating SMOS ocean surface salinity in the Atlantic with Argo and operational ocean model data. *IEEE Transactions on Geoscience and Remote Sensing*, **50**(5): 1 688-1 702.

Boutin J, Martin N, Yin X, Reul N, Spurgeon P. 2012. First assessment of SMOS measurements over open ocean: part II Sea Surface Salinity. *IEEE Transactions on Geoscience and Remote Sensing*, **50**(5): 1 648-1 661.

Camps A, Font J, Vall-llosera M, Gabarró C, Corbella I, Duffo N, Torres F, Blanch S, Aguasca A, Villarino R, Enrique L, Miranda J J, Arenas J, Juliá A, Etcheto J, Caselles V, Weill A, Boutin J, Contardo S, Niclós R, Rivas R, Reising S C, Wursteisen P, Berger M, Martín-Neira M. 2004. The WISE 2000 and 2001 field experiments in support of the SMOS mission: sea surface L-band brightness temperature observations and their application to sea surface salinity retrieval. *IEEE Transactions on Geoscience and Remote Sensing*, **42**(4): 804-823.

Dinnat E P, Boutin J, Caudal G, Etcheto J. 2003. Issues concerning the sea emissivity modeling at L band for retrieving surface salinity. *Radio Science*, **38**(4).

Dinnat E P, Boutin J, Caudal G, Etcheto J, Waldteufel P. 2002. Influence of sea surface emissivity model parameters in L-band for the estimation of salinity. *International Journal of Remote Sensing*, **23**(23): 5 117-5 122.

Durden S L, Vesecky J F. 1985. A physical radar cross-section model for a wind-driven sea with swell. *IEEE Journal of Oceanic Engineering*, **OE-10**(4): 445-451.

Font J, Camps A, Borges A, Martín-Neira M, Boutin J, Reul N, Kerr Y H, Hahne A, Mecklenburg S. 2010. SMOS: the challenging sea surface salinity measurement from space. *Proceedings of the IEEE*, **98**(5): 649-665.

Gabarró C, Font J, Camps A, Vall-llosera M, Juliá A. 2004. A new empirical model of sea surface microwave emissivity for salinity remote sensing. *Geophysical Research Letters*, **31**(1): L01309-1-L01309-5.

Irisov V G. 1997. Small-slope expansion for thermal and reflected radiation from a rough surface. *Waves Random Media*, **7**(1): 1-10.

Johnson J T, Zhang M. 1999. Theoretical study of the small slope approximation for ocean polarimetric thermal emission. *IEEE Transactions on Geoscience and Remote Sensing*, **37**(5): 2 305-2 316.

Kudryavtsev V N, Makin V K, Chapron B. 1999. Coupled sea surfaceatmosphere model-Part 2: spectrum of short wind waves. *Journal of Geophysical Research*, **104**(C4): 7 625-7 639.

Martín-Neira M, Goutoule J M. 1997. MIRAS — a two-dimensional aperture synthesis radiometer for soil moisture and ocean salinity observations. *ESA Bulletin*, **2**: 95-104.

Mcmullan K D, Brown M A, Martin-Neira M, Rits W, Ekholm S, Marti J, Lemanczyk J. 2008. SMOS: the payload. *IEEE Transactions on Geoscience and Remote Sensing*, **46**(3): 594-605.

Reul N, Chapron B. 2003. A model of sea foam thickness distribution for passive microwave remote sensing applications. *Journal of Geophysical Research Oceans*, **108**(C10).

Reul N, Chapron B, Mevel S, Le Traon P-Y, Obligis E, Boone C, Bahurel P, Brasseur P, Testut C-E, Tranchant B, Font J, Gabarró C, Srokos, M, Snaith H, Gommenginger C, Camps A, Vall-llosera M, Miranda J, Sabia R, Germain O, Soulat F, Bertino L, Le Vine D M, Lagerloef G S E. 2006. Synergetic Aspects and Auxiliary Data Concepts for Sea Surface Salinity Measurements from Space. European Space Agency ESTEC Contract 18176/04/NL/CB, Final Report.

Reul N, Tenerelli J, Boutin J, Chapron B, Paul F, Brion E, Gaillard F, Archer O. 2012. Overview of the first SMOS sea surface salinity products. Part I: quality assessment for the second half of 2010. *IEEE Transactions on Geoscience and Remote Sensing*, **55**(5): 1 636-1 647.

Subrahmanyam B, Grunseich G, Nyadjro E S. 2013. Preliminary SMOS salinity measurements and validation in the Indian Ocean. *IEEE Transactions on Geoscience and Remote Sensing*, **51**(1): 19-27.

Wentz F. 1975. A two-scale model for foam-free sea microwave brightness temperature. *Journal of Geophysical Research*, **80**(24): 3 441-3 446.

Yin X, Boutin J, Martin N, Spurgeon P. 2012. Optimization of L-Band sea surface emissivity models deduced from SMOS Data. *IEEE Transactions on Geoscience and Remote Sensing*, **50**(5): 1 414-1 426.

Yueh S H. 1997. Modeling of wind direction signals in polarimetric sea surface brightness temperatures. *IEEE Transactions on Geoscience and Remote Sensing*, **35**(6): 1 400-1 418.

Zin S, Boutin J, Font J, Reul N, Waldteufel P, Gabarró C, Tenerelli J, Petitcolin F, Vergely J L, Talone M, Delwart S. 2008. Overview of the SMOS sea surface salinity prototype processor. *IEEE Transactions on Geoscience and Remote Sensing*, **46**(3): 621-645.